Numerical Determination of the Topological Properties of the Electronic Charge Density in Molecules and Solids Using Density Functional Theory

Yosslen Aray,* Jesús Rodríguez, and Juan Rivero

Centro de Química, IVIC, Apartado 21827, Caracas 1020A, Venezuela

Received: April 16, 1997; In Final Form: July 7, 1997[⊗]

A numerical method to analyze the topology of the electronic density regardless of how it was obtained (analytically or numerically) was implemented for the Extreme 94 program. The method allows the study of a complex system by density functional theory where the electronic correlation is important, regardless of the kind of basis set used, and allows the analysis of the resulting charge density with the topological theory of Bader.

1. Introduction

Density functional theory (DFT) plays a role of increasing importance in the calculations of ground states of molecules and solids.[1−9] The inclusion of the electron correlation effects is necessary for an accurate description of many-electron systems.[2] By standard methods such as configuration interaction, perturbation, or Green's function theory, the inclusion of the electron correlation for an extended system is a very difficult matter.[2] However, this problem is lessened with the appearance of DFT, in which the correlation is included by introducing a local (or nonlocal) approximation for a functional of the electronic density that describes the correlation effects. The practical implementations of DFT lead to the Kohn and Sham (KS) equations.[2] Their solution allows us to handle complex systems such as solids, surfaces, interfaces, transition metals, and organometallic compounds.[6,8] Additionally, DFT methods are not restricted to traditional Gaussian basis set functions[6] since it is possible to use different basis sets such as muffin tin orbitals, multiple scattering, plane waves, or numerical functions.

The topological theory of Bader et al. is very useful to extract the chemical information from the charge density.[10−21] A recent study,[22] using molecular orbital Hartree−Fock, post-Hartree−Fock at MP2 and QCISD levels, and DFT calculations, has confirmed that the DFT methods provide a good description of the topology of the electronic density, $\rho(\mathbf{r})$. Unfortunately, the available algorithms for the topological analysis of $\rho(\mathbf{r})$ (EXTREME,[23] Gaussian 94,[24,25] MORPHY,[26] and TOPOND[27] program in Crystal 95[28]) have been usually implemented for analytical Gaussian basis sets. To our knowledge, only one case (Guo[29] et al. performed DF calculations and topological analysis of the charge density on Ni clusters using a purely numerical basis set) of a nonanalytical basis set exists. This limits the applicability of the topological analysis of $\rho(\mathbf{r})$ in many interesting systems in which the correlation effects play an important role. Due to the existence of a large variety of software employing different basis sets and the unavailability of the source code in commercial cases, in the present work, a numerical method that is able to analyze the topology of the electronic density regardless of how it was generated (analytically or numerically) is described. The method allows one to study complex systems by DFT regardless of the basis set used and to analyze the resulting density with the topological theory of Bader. In the present study, this method was implemented as a modification to the EXTREME 94[23] program and applied to CO, NaF, NO, and HCCH molecules, Na_4F_4, Cu_{13}, and Cu_{45} clusters plus Cu bulk. Cu_{45} was studied with DMOL[30] program using a numerical basis set while Cu bulk was studied with WIEN 95[31] program using muffin tin orbitals and plane waves. The other systems were done with GAUSSIAN 94 using an analytical Gaussian basis set.

2. Theory

The topological properties of a molecular charge distribution are summarized by its critical points (CP).[10] These are points where the gradient vector field, $\nabla\rho(\mathbf{r})$ vanishes, and they are classified by the $\rho(\mathbf{r})$ curvatures or three eigenvalues λ_i ($i = 1$, 2, and 3) of the Hessian matrix ($H_{ij} = \partial^2\rho(\mathbf{r})/\partial x_i\,\partial x_j$). There are, in molecules and crystals, four types of these extremes that are labeled by their rank (number of nonzero eigenvalues) and signature (excess number of positive over negative eigenvalue). These are maxima (3,−3), minima (3,+3), and saddle points (3,+1) and (3,−1). The (3,−3) points occur generally at the nuclear positions so that each nucleus is a three-dimensional point attractor in the vector field $\nabla\rho(\mathbf{r})$. The region traversed by the gradient paths which terminate at a given attractor is called the *basin* of the attractor. A (3,−1) CP is found between every pair of neighboring nuclei. It represents both local maxima in two directions and a local minimum in a third and is called a *bond critical point*. The gradient paths associated with the negative eigenvalues at the (3,−1) point define the zero-flux surfaces that partition the molecule or crystal into unique fragments. Therefore, the set of surfaces formed by all (3,−1) points partitions the system into a collection of chemically identifiable regions called atomic basins.[32] These are the most transferable pieces one can define in an exhaustive partitioning of the real space.[10] The unique pair of trajectories associated with the positive eigenvalue at the (3,−1) point define a line linking the nuclei, along which the charge density is a maximum with respect to any neighboring line. It is called a *bond path*, and its presence provides the necessary and sufficient conditions for the existence of a bond.[10] The network of bond paths defines a graph that describes the structure of a molecules or a crystal. A bond path determines and characterizes all of the atomic interactions in a given system[15,16] and has proven useful in the analysis of physical properties of insulators, pure metals, and alloys.[15−18] The bond path provides a general concept of a chemical bond in ionic, covalent, metallic, and van der Waals solids, allowing the definition of a novel theory[17] of cohesion and adhesion.

3. Methodology

Extreme 94[23] determines the critical points of $\rho(\mathbf{r})$ based on the Newton−Raphson (NR) technique.[33] The NR algorithm starts from a truncated Taylor expansion at a point $\mathbf{r} = \mathbf{r}_0 + \mathbf{h}$, about $\mathbf{r}_0$ of a multidimensional scalar function:

$$\rho = \rho_0 + \mathbf{g}^T\mathbf{h} + {}^1/_2\mathbf{h}^T\mathbf{H}\mathbf{h} \qquad (1)$$

* E-mail: yaray@quimica.ivic.ve.

[⊗] Abstract published in *Advance ACS Abstracts,* August 15, 1997.

S1089-5639(97)01325-X CCC: $14.00

TABLE 1: Topological Properties (au) of $\rho(r)$ at the Bond Critical Point for the CO and NaF Molecules

CO

step[a]	r_C[b]	$\lambda_1 = \lambda_2$	λ_3	$\rho(r_c)$	$\nabla^2\rho(r_c)$
analytic	0.736 722 61	−1.555 016 47	3.491 418 99	0.478 741 35	0.381 386 05
0.04	0.736 748 29	−1.565 560 36	3.488 143 44	0.478 745 09	0.357 022 73
	0.736 721 91	−1.554 884 43	3.491 625 10	0.478 741 26	0.381 856 25
	0.736 722 30	−1.555 018 70	3.491 423 54	0.478 741 35	0.381 386 14
0.03	0.736 751 10	−1.570 343 16	3.480 072 47	0.478 745 44	0.339 386 14
	0.736 722 93	−1.555 287 06	3.491 217 30	0.478 741 37	0.380 673 19
	0.736 722 57	−1.555 016 68	3.491 419 77	0.478 741 35	0.381 386 41
0.02	0.736 720 30	−1.557 260 29	3.496 655 79	0.478 743 85	0.382 135 20
	0.736 723 18	−1.555 146 86	3.491 307 04	0.478 741 35	0.381 013 32
	0.736 722 61	−1.555 016 52	3.491 418 99	0.478 741 35	0.381 385 99

NaF

step[a]	r_{Na}[b]	$\lambda_1 = \lambda_2$	λ_3	$\rho(r_c)$	$\nabla^2\rho(r_c)$
analytic	1.723 673 96	−0.071 214 25	0.533 838 32	0.04792425	0.391 409 82
0.04	1.723 464 2 9	−0.066 987 30	0.538 054 31	0.047 922 16	0.404 079 71
	1.723 675 48	−0.071 180 99	0.533 888 10	0.047 924 24	0.391 526 13
	1.723 673 95	−0.071 214 25	0.533 838 29	0.047 924 25	0.391 409 81
0.03	1.723 355 79	−0.061 971 24	0.547 506 08	0.047 920 09	0.423 563 60
	1.723 671 16	−0.071 219 09	0.533 99 265	0.047 924 22	0.391 554 47
	1.723 673 96	−0.071 214 25	0.533 83 829	0.047 924 25	0.391 409 78
0.02	1.723 099 62	−0.046 304 05	0.550 428 62	0.047 919 96	0.457 820 52
	1.723 677 31	−0.071 524 58	0.533 791 15	0.047 924 25	0.390 741 97
	1.723 673 96	−0.071 214 25	0.533 838 29	0.047 924 25	0.391 409 80

[a] The properties were calculated using ρ stored with 5, 7, and 12 figure numbers for first, second, and third row, respectively. The analitical values were calculated with EXTREME 94 and the others with the EXCUBO program**.** In each case ρ was determined using KOs orbitals calculated with GAUSSIAN 94 and a 6-31G** basis set. [b] r_C and r_{Na} are the distances from the critical point to the C or Na atom, respectively.

TABLE 2: Topological Properties (au) of $\rho(r)$ at the Bond Critical Point for the NO, and HC≡CH Molecules

NO

step	r_N[b]	λ_1	λ_2	λ_3	$\rho(r_c)$	$\nabla^2\rho(r_c)$
analytic	0.920 171 09	−1.470 061 68	−1.376 216 93	1.131 338 30	0.562 513 69	−1.714 940 31
0.04	0.920 171 46	−1.470 013 53	−1.376 226 61	1.131 445 34	0.562 513 65	−1.714 794 80
	0.920 171 00	−1.470 061 74	−1.376 216 90	1.131 337 77	0.562 513 69	−1.714 940 87
0.03	0.920 172 33	−1.470 071 18	−1.37 6339 07	1.131 210 22	0.562 513 75	−1.715 200 03
	0.920 171 08	−1.470 061 68	−1.376 216 93	1.131 338 15	0.562 513 69	−1.714 940 47
0.02	0.920 168 99	−1.470 002 57	−1.376 399 03	1.131 922 24	0.562 513 70	−1.715 479 37
	0.920 171 09	−1.470 061 68	−1.376 216 93	1.131 338 34	0.562 513 69	−1.714 940 27

HCCH C−C bond

step[a]	r_C[b]	$\lambda_1 = \lambda_2$	λ_3	$\rho(r_c)$	$\nabla^2\rho(r_c)$
analyytic	1.133 228 28	−0.673 762 47	0.106 230 10	0.411 756 18	−1.241 294 81
0.04	1.133 228 26	−0.673 891 69	0.106 101 69	0.411 756 20	−1.244 168 17
	1.133 228 28	−0.673 762 47	0.106 230 08	0.411 756 18	−1.241 294 83
0.03	1.133 228 26	−0.673 675 80	0.106 22111	0.411 756 20	−1.241 130 45
	1.133 228 28	−0.673 762 47	0.106 230 08	0.411 756 18	−1.241 294 83
0.02	1.133 228 26	−0.673 468 65	0.105 880 16	0.411 756 20	−1.241 057 14
	1.133 228 28	−0.673 762 47	0.106 230 09	0.411 756 18	−1.241 294 81

[a] The properties were calculated using ρ stored with 7 and 12 figure numbers for first, and second row, respectively. The analytical values were calculated with EXTREME−94 and the others with the EXCUBO program**.** In each case ρ was determined using KOs orbitals calculated with GAUSSIAN 94 and a 6-31G** basis set. [b] r_N and r_C are the distances from the critical point to the N or C atom, respectively.

TABLE 3: Topological Properties (au) of $\rho(r)$ at the Critical Points[a,b] for One of the Regular Tetrahedron in Na_4F_4

	r_A[c]	λ_1	λ_2	λ_3	$\rho(r_c)$	$\nabla^2\rho(r_c)$
Na-F	1.891 329 80	−0.035 891 14	−0.035 745 33	0.256 832 39	0.027 479 43	0.185 195 92
	1.891 329 78	−0.035 891 19	−0.035 745 70	0.256 833 23	0.027 479 43	0.185 196 33
F-F	2.904 234 32	−0.006 244 56	−0.000 924 76	0.038 281 11	0.008 555 22	0.031 111 79
	2.904 234 32	−0.006 244 26	−0.000 924 56	0.038 281 77	0.008 555 22	0.031 111 94
ring		−0.006 325 72	0.001 900 57	0.037 082 21	0.008 543 42	0.032 657 06
NaFF		−0.006 326 16	0.001 900 21	0.037 081 91	0.008 543 42	0.032 655 90
cage		0.005 071 24	0.005 071 24	0.005 071 24	0.003 817 78	0.015213 73
		0.005 071 14	0.005 071 14	0.005 071 14	0.003 817 78	0.015 213 42

[a] Critical points are labeled by rank, number of nonzero λ_i, and signature, sum of algebraic signs of λ_i. A bond critical point is (3,−1), ring (3,+1) and cage (3,+3). [b] In each line, the first and second rows give the EXTREME and EXCUBO ($h = 0.04$ au and FN = 12) results, respectively. In each case ρ was determined using KOs orbitals calculated with GAUSSIAN 94 and a 6-311+G(d,p) basis set. [c] r_A is the distances from the critical point to the left atom of the bond.

where ρ is the charge density and **g** and **H** are the gradient and Hessian (matrix) at point $\mathbf{r}_0$, respectively. The best step **h** to get from the initial $\mathbf{r}_0$ to the critical point is $\mathbf{h} = -\mathbf{H}^{-1}\mathbf{g}$**.** This correction is then used to obtain a vector $\mathbf{r}_{new}$ and the process is iterated to $\nabla\rho(\mathbf{r}) = \mathbf{0}$. The NR algorithm requires the evaluation of the first and second partial derivatives of ρ, at arbitrary points **r**. The EXTREME 94 program evaluates these derivatives analytically, using a Gaussian basis representation for the electronic density.

In the present work, we project ρ onto a homogeneous grid of interval size h and use standard numerical methods[33] to calculate the partial derivatives of ρ, which are then used in the NR algorithm. In a simple approach, we have used finite difference approximations to the first and second derivatives, for equally spaced base points. We have developed derivative expressions with sixth-order error ($O(h^6)$) and backward, forward, and central interpolation. For example, using the stencil form,[33] centered-difference approximation formulas, to determine the noncrossed first and second derivatives of ρ and the mixed partial derivatives such as $\partial^2\rho/\partial x\,\partial y$ (due to the fact that the sixth-order expression is just too large to fit the page,

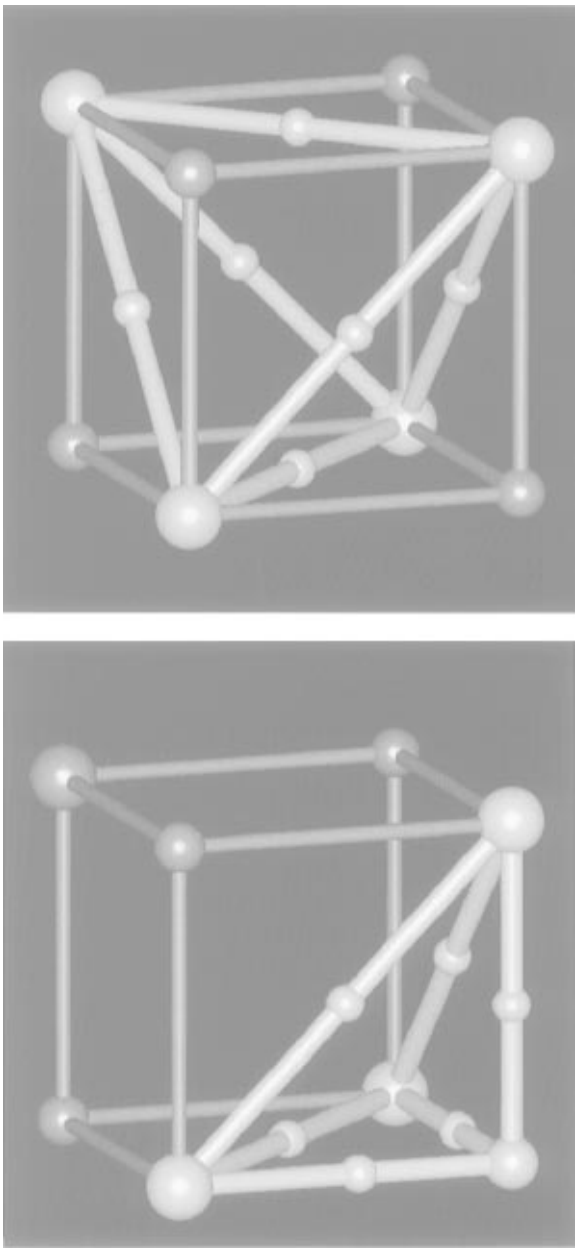

Figure 1. Na_4F_4 cluster. Large and medium spheres denote Na and F atoms while the small ones mark the bond critical points. The structure defined by the cluster graph results from packing one F_4 graph similar to that highlighted in (a, top) and four NaF_3 graphs as that highlighted in the right corner of (b, bottom).

we have chosen one with an error of $O(h^3)$ as illustrative) are

$$\frac{\partial \rho}{\partial \omega} = \frac{1}{60h}\left(\underset{-1}{\bigcirc}\!\!-\!\!\underset{9}{\bigcirc}\!\!-\!\!\underset{-45}{\bigcirc}\!\!-\!\!\underset{0}{\bigcirc}\!\!-\!\!\underset{45}{\bigcirc}\!\!-\!\!\underset{-9}{\bigcirc}\!\!-\!\!\underset{1}{\bigcirc}\right) \quad (2)$$

$$\frac{\partial^2 \rho}{\partial \omega^2} = \frac{1}{180h^2}\left(\underset{2}{\bigcirc}\!\!-\!\!\underset{-27}{\bigcirc}\!\!-\!\!\underset{270}{\bigcirc}\!\!-\!\!\underset{-490}{\bigcirc}\!\!-\!\!\underset{270}{\bigcirc}\!\!-\!\!\underset{-27}{\bigcirc}\!\!-\!\!\underset{2}{\bigcirc}\right) \quad (3)$$

$$\frac{\partial^2 \rho}{\partial \omega \partial \beta} = \frac{1}{12h}\begin{pmatrix} -1 \\ 8 \\ 0 \\ -8 \\ 1 \end{pmatrix}\begin{pmatrix} 1 & -8 & 0 & 8 & -1 \end{pmatrix}\frac{1}{12h} = \frac{1}{12^2h^2}\begin{Bmatrix} -1 & 8 & 0 & -8 & 1 \\ 8 & -64 & 0 & 64 & -8 \\ 0 & 0 & \underset{0}{\bigcirc} & 0 & 0 \\ -8 & 64 & 0 & -64 & 8 \\ 1 & -8 & 0 & 8 & -1 \end{Bmatrix} \quad (4)$$

Such expressions include only the coefficients of the functional

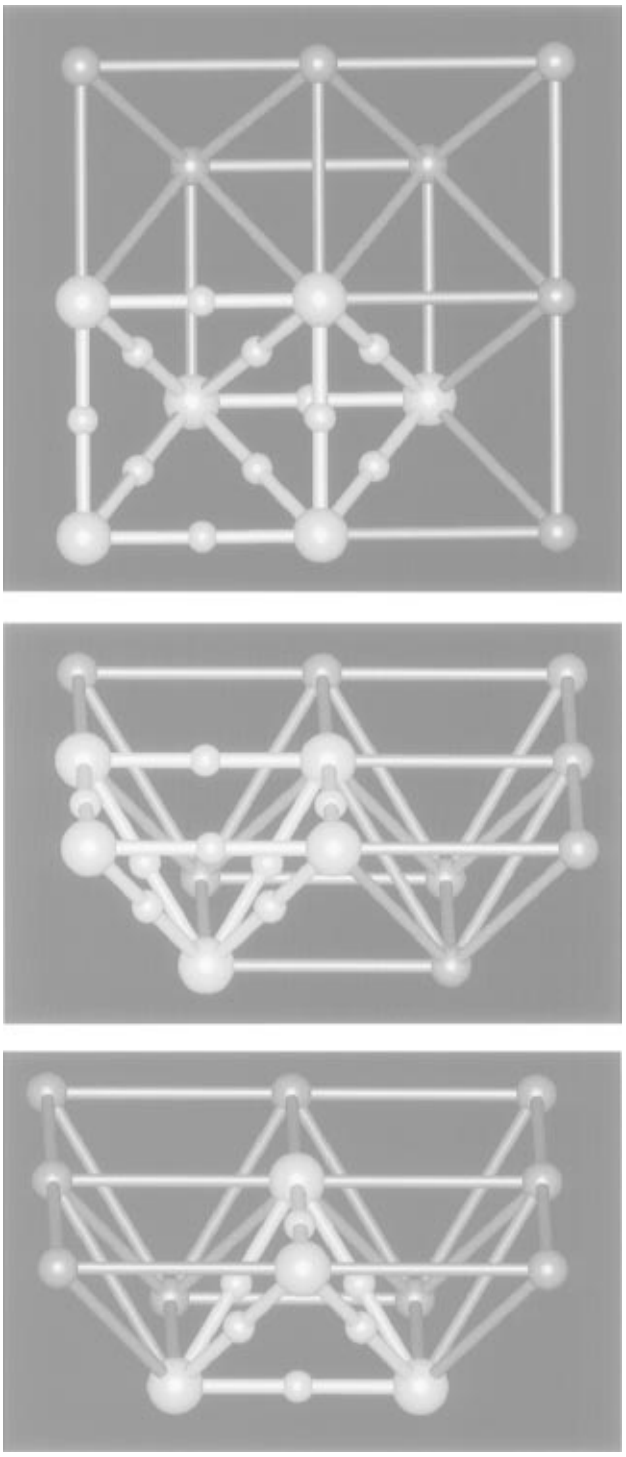

Figure 2. Cu_{13} cluster modeling a (100) Cu surface. (a, top) Top view. (b, middle) Side view with the graph of one inverted square pyramid highlighted. (c, bottom) Side view highlighting the graph of one tetrahedron. The structure results from packing four square pyramids and four regular tetrahedra between them. The small white spheres denote the bond critical points.

values present in the derivative formulas. The double circles indicate the position of the base point where the derivative is being evaluated and the adjacent circles are separated by the interval h.

Our methodology consists of performing all calculations as though the electronic density was on a uniform grid. If the source code is available, we work on a virtual grid and the program evaluates ρ only at the necessary points. That is, the values of ρ need not be stored and need only be calculated at the appropriate points. If the source code is unavailable, a grid

TABLE 4: Topological Properties (au) of $\rho(r)$ at the Critical Points[a,b] for One of the Square Pyramid in the Cu_{13} Cluster

Bond[c]						
A−B	r_A	λ_1	λ_2	λ_3	$\rho(r_c)$	$\nabla^2\rho(r_c)$
C-B	2.414 370 0	−0.028 911 2	−0.027 158 2	0.143 707 5	0.031 245 8	0.087 638 2
B-B	2.42 9048 7	−0.031 117 9	−0.028 669 9	0.137 123 3	0.031 099 4	0.07 7335 4
C-D	2.424 047 1	−0.028 231 6	−0.025 660 9	0.144 508 9	0.031 693 2	0.090 616 4
B-D	2.422 122 0	−0.028 971 0	−0.026 348 3	0.141 9806 9	0.030 947 5	0.086 661 4
B-D	2.434 190 9	−0.029 993 2	−0.028 447 2	0.134 5724 1	0.031 572 6	0.076 13 20

Rings					
ABC	λ_1	λ_2	λ_3	$\rho(r_c)$	$\nabla^2\rho(r_c)$
C-D-B	−0.011 293 9	0.038 536 1	0.0406487	0.0203799	0.0678909
B-C−B	−0.014 761 1	0.038 210 3	0.0402063	0.0199296	0.0636556

[a] See footnote *a* of Table 3. [b] In this case, with a presicion of 7 significant figures, EXTREME and EXCUBO ($h = 0.04$ au and FN = 12) give exactly the same results. ρ was determined using KOs orbitals calculated with GAUSSIAN 94 and a 6-311+G(d,p) basis set. [c] C, D, B denote central, lower, and border atoms on the square pyramid (see Figure 2).

TABLE 5: Topological Properties (au) of $\rho(r)$ at the Critical Points for Bulk Cu *Fm*3*m* (No. 225)

Wyckoff letter[a]	critical point	λ_1	λ_2	λ_3	$\rho(r_c)$	$\nabla^2\rho(r_c)$
e 24	Cu−Cu bond	−0.0233	−0.0180	0.1339	0.0403	0.0926
f 32	ring	−0.0074	0.0175	0.0175	0.0338	0.0275
b 4	octahedral cage	0.0134	0.0134	0.0134	0.0222	0.0402
c 8	tetrahedral cage	0.0064	0.0064	0.0064	0.0332	0.0193

[a] Except for the cage, the octahedra and tetrahedra graphs have exactly the same value for the remainder critical points.

of stored values of ρ must be prepared. In this case, the computational load can be larger than that required by the analytical approaches. Once that grid is built, one needs to calculate the derivatives of ρ at the same number of arbitrary points $\mathbf{r}_i$ in both methods. The analytical method calculates the values of the derivatives only at the $\mathbf{r}_i$ points using the basis functions while the numerical method uses equations such as (2)−(4). Such equations involve several points around each $\mathbf{r}_i$, and our program has to interpolate when the points are not on the grid. Thus, when the code is unavailable, the additional computational load of the proposed method corresponds to the number of points on the grid where ρ has to be calculated plus the interpolation at the points that are not on that grid.

4. Results and Discussion

The accuracy of the numerical evaluation of the topological properties of the $\rho(\mathbf{r})$ at the critical points with the modified version of EXTREME 94 (that we call EXCUBO) was tested by comparing the results of Gaussian 94 analytic KSOs (Kohn−Sham orbitals) using the original EXTREME 94 program, and the results using a numerical grid of ρ, calculated with the CUBEV program of the AIMPAC 94 package.[23] CUBEV builds a homogeneous grid of ρ of step size h. The analytic KSOs were calculated using the gradient-corrected Becke exchange potential[34] together with the correlation potential of Lee, Yang, and Parr[35] (BLYP) and the 6-311G Gaussian basis set.[36] An error of order of h^6 is expected for the first and second derivatives associated with the difference approximation used. Therefore, for h around 0.03 au a precision of 10^{-12} au should be expected. However, this also depends on the precision of the calculation and, when the grid is built, of the number of figures used by commercial software in the storage of the density. This is an important point because in most of the software currently used, the density is stored only for plotting purposes with three to five significant figures (FN).

To study the effect of the size of h and FN of ρ on the localization and topological properties at the critical points of ρ, we have analyzed the bond critical point in CO and NaF molecules using different values of h and ρ. The results of the distance from the critical points to the A atom, $\mathbf{r}_A$, the perpendicular curvatures to the bond path, λ_1 and λ_2, the parallel curvatures to the bond path, λ_3, the density value, $\rho(\mathbf{r_c})$, and Laplacian, $\nabla^2\rho(\mathbf{r_c})$, for selected h values and FN levels used in the storage of ρ, are given in Table 1. Clearly, the properties converge toward the analytic results only when ρ is given with 12 significant figures. In this case, a step size of $h = 0.04$ au is enough to obtain a precision of 6 FN in all the calculated properties. However, we can also see that the storage of ρ with a FN value between 7 and 12 guarantees a precision from 4 to 6 FN in the topological analysis of ρ. A FN equal to 5, on the other hand, allows the localization of the critical point and the correct determination of its type, (3,−1) while the remaining properties are not well reproduced, i.e., it generates results of qualitative value only.

In a second example, we have done a similar study on the NO and HCCH molecules. The ground state of NO (Π^2) has the open-shell configuration $(1\sigma)^2(2\sigma)^2(3\sigma)^2(4\sigma)^2(5\sigma)^2(1\pi)^4(2\pi)$ so that the extra electron in the 2π molecular orbital, that is mostly localized in a plane, destroys the axial symmetry and $\lambda_1 \neq \lambda_2$. The results for a FN of 7 and 12 in ρ are collected in Table 2. They confirm that a value of h around 0.03 au and a FN of 12 in ρ produces a good precision (around 10^{-7} au) in the location and the topological properties at the critical points of ρ.

To consider more complex cases, we have studied also the Na_4F_4 and Cu_{13} clusters. Na_4F_4 is a small model of the bulk NaF ionic solid. The most stable phase[37] of NaF is a cubic fcc and belongs to the *Fm*3*m* space group with $a = 4.62$ Å. In Na_4F_4 (see Figure 1), in addition to the Na−F bonds, we found bond critical points between the F atoms so that each Na atom forms a regular tetrahedron with its three closest F neighbors, which in turn form a regular tetrahedron between themselves. The structure of this cluster is the result of packing four NaF_3 and one F_4 regular tetrahedra. The graph of one of these tetrahedra is also shown in Figure 1. The results obtained for that graph with a value of $h = 0.04$ au are collected in Table 3. The number and type of critical points defining the graph (four nuclear attractors, four bond critical points, two four-membered rings, and one cage) obey the Poincaré−Hopf[10] relationship for a stable structure of molecules or cluster, $n - b + r - c = 1$, where n, b, r, and c are the numbers of nuclear attractors, bond, ring, and cage critical points, respectively.

Cu_{13} (Figure 2) is a model of the Cu (100) surface with the geometrical parameters of the bulk. Previous results[22] have shown that the structure of that cluster is a truncated form of that found for the bulk Cu with bond paths linking each surface

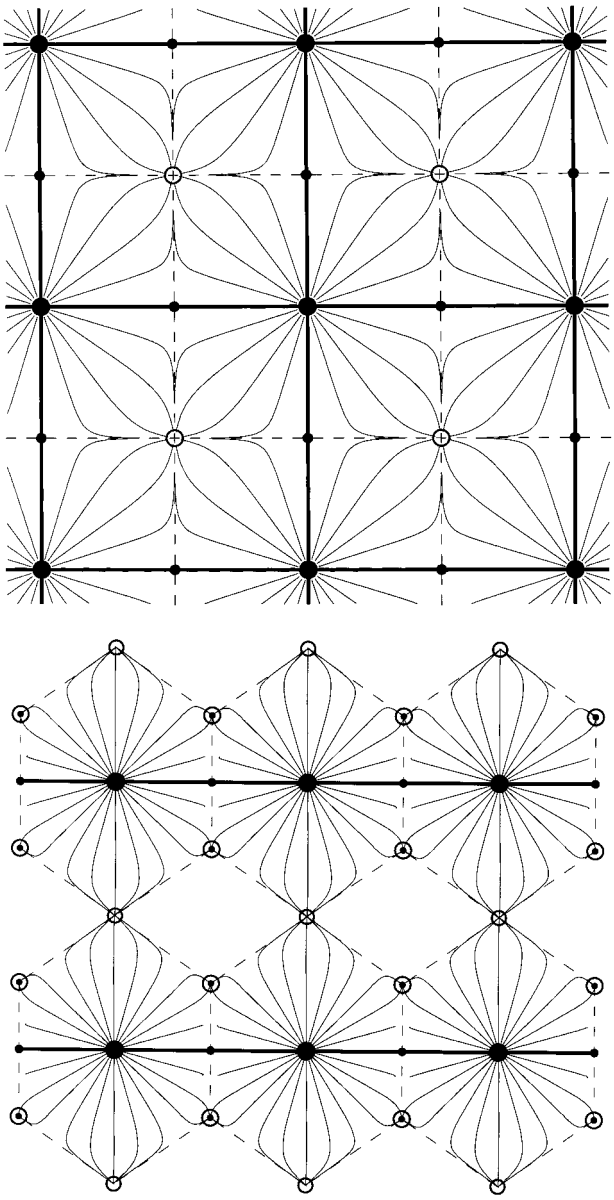

Figure 3. Trajectories traced out by gradient vectors of the electron density calculated using WIEN 95 program: trajectories of $\nabla\rho(\mathbf{r})$, in the (100) (a, top) and (110) (b, bottom) planes of Cu. The region of space traversed by trajectories that terminate at a given nucleus (denoted by a large filled dots) where $\rho(\mathbf{r})$ is a local maximum, defines the basin of the atom. Each atom is bounded by sets of trajectories that terminate at (3,−1) or bond critical point (denote by small filled dots). Only one pair from such a set, indicated by dotted lines, appears for each bond critical point in (a) and (b). A unique pair of trajectories also originates at each bond critical point defining a line of maximum electron density linking bonded nuclei, the bond path, as also indicated in (a) and (b). The remaining critical points in those planes are (3,+3) or cage critical points located in the octahedral holes (denote by open dots) and the tetrahedral holes (denoted by a dot inside a circle).

Cu atom to its first neighbors. The top atoms form square pyramids (in slabs of three or more layers the top atoms are capping octahedra) with the lower atoms and tetrahedra between them which at the same time form inverted square pyramids. Each of those tetrahedra is capped by a bond path on the first layer of atoms. The graph of one of the inverted square pyramids and tetrahedron are also shown in Figure 2 and the topological properties of ρ at the critical points for $h = 0.04$ au are collected in Table 4. In accordance with the Poincaré−Hopf relationship there are eight bond critical points and four three-membered rings for the five nuclear attractors forming the square-pyramid graph. Tables 3 and 4 show that, even in these complex cases, a value of h around 0.03 au and 12 FN (in principle, if one had access to the source code, the computational cost could be independent of FN; however, if this is not the case, one pays for one's decimals) on ρ offer a good compromise between computational cost and numerical precision (around 10^{-6}) in the location of the critical points and the calculations of the topological properties of the electronic density at these sites.

The previous results show that EXCUBO can be applied with confidence to any numeric density regardless of the method employed in its determination. As an example of its capabilities, we will apply it to calculate the topological properties of electronic densities determined using two very different methods of solving the KS equations and different atomic basis sets. In this final application, we will investigate the topological properties of ρ and the crystal structure of the Cu bulk and the Cu (100) surface. The bulk was studied using the WIEN 95 program and the correlation and exchange functional of Perdew et al.[38] to generate ρ. That program uses the full-potential linearized-augmented-plane-wave (FLAPW) method,[39] which is among one of the most accurate methods available for energy band-structure calculations. In the FLAPW method the unit cell is divided into nonoverlapping spheres (with radii R_i) and in interstitial regions; in the former region the wave function is expressed in atomic-like functions and in the latter region in plane waves. The charge density inside the spheres is written as a linear combination of radial functions multiplied by symmetrized spherical harmonics $Y_{\mathrm{lm}}(\mathbf{r})$ and as a Fourier series in the interstitial region. The source code is available so the grid storage and computation is not required.

The most stable phase of bulk Cu is cubic fcc[40] and belongs to the *Fm*3*m* space group with $a = 3.577$ Å. Each atom has 12 nearest neighbors at 2.56 Å. Previous studies[17,41] have found bond critical points midway between nearest neighbors suggesting the formation of two types of polyhedra sharing its faces: octahedra and tetrahedra with a cage critical point at the center and eight- and four-ring critical points at the faces, respectively. However, that study reported only the topological properties of the charge density at the bond critical point. In the present work we have located all CPs and the parameters that characterize them are given in Table 5. Table 5 identifies the critical points within a unit cell with the corresponding Wyckoff letter in the *International Tables for Crystallography*,[42] which serve as an aid in determining the topology of the electron density of an extended system. Additionally, the topologically defined elements of the Cu bulk structure are illustrated in Figures 3 and 4. The results confirm that the crystal graph of the bulk Cu is the result of packing octahedra and tetrahedra. Those graphs for a Cu unit cell are also shown in Figure 4.

The Cu (100) surface was studied using the Cu_{41} cluster modeling a periodic slab of two layers and the DMOL program to generate ρ. This program uses the method of linear combinations of atomic orbitals, or LCAO method to solve the KS equations. A set of atomic numerical orbitals,[30] given as values on an atomic-centered spherical-polar mesh, are used as a basis set so the KS orbitals and ρ are numerical functions. In this case, a grid-based plot of ($h = 0.03$ au and FN of 10) was built using the BLYP functional and a double-numerical basis set (DNP).[30] The Cu_{41} cluster, unlike Cu_{13}, allows one to model the polyhedra that form the structure of the surface without nuclear attractors in the border. Thus, we have found that in Cu_{41}, the set of CPs that define those tetrahedra previously mentioned, have the right symmetry for the graph of the periodic slab, i.e., C_{4v} in the cluster model and *P*4*mm* in the slab. The topological properties at the CPs that generated the tetrahedra

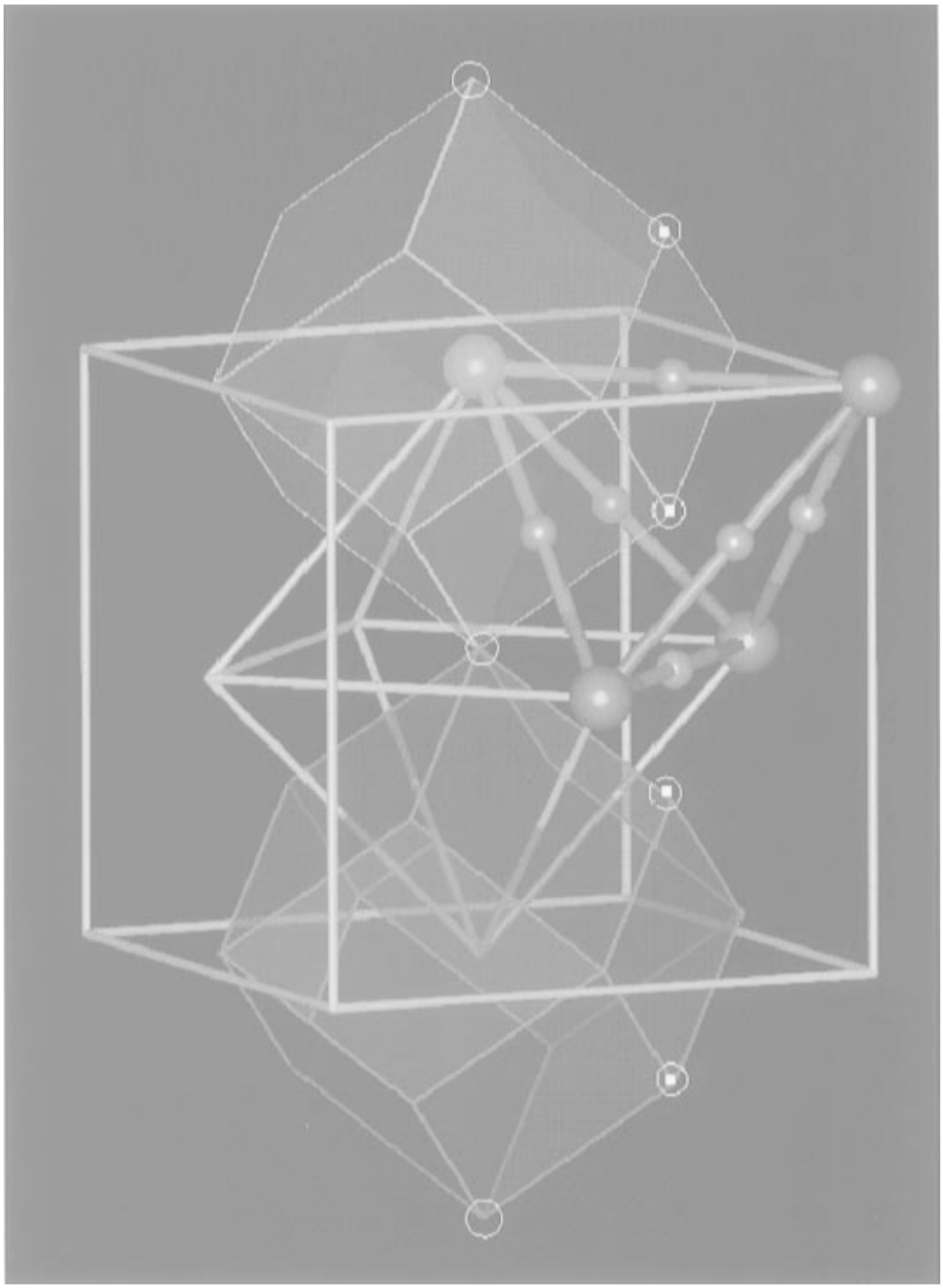

Figure 4. Crystal graph characteristic of the Cu fcc topology. The white cube denotes the unit cell. Blue and pink spheres mark, respectively, the Cu atoms and the bond critical points defining one of the tetrahedral graphs. There are in the cell eight tetrahedra similar to that, sharing one face with the central octahedral graph. Additionally, the basin (just the Wigner−Seitz cell) of two atoms, denoted by yellow and green regions, are superposed to show in 3D the topological structure elements of $\rho(\mathbf{r})$ drawn in Figure 3 on the (110) plane. Open circles mark the octahedral cage critical points while a square inside a circle denotes a tetrahedral cage critical point.

TABLE 6: Topological Properties (au) of $\rho(r)$ at the Critical Points for One Central Tetrahedron in the Cu_{41} Cluster

critical point	λ_1	λ_2	λ_3	$\rho(r_c)$	$\nabla^2\rho(r_c)$
Cu−Cu in layer	−0.0255	0.0227	0.1234	0.0440	0.0752
Cu−Cu between layers	−0.0322	0.0265	0.1583	0.0500	0.0997
ring	−0.0121	0.0285	0.0393	0.0390	0.0558
cage	0.0134	0.0180	0.0192	0.0378	0.0506

(five bond critical points, four three-membered rings, and one four-membered cage) are collected in Table 6. Despite the very different methods used to determine the electronic density in the bulk and cluster cases, the values of the parameters for the bond critical points on the slab are extraordinarily similar to the bulk ones. The most interesting changes in the BCP parameters from bulk to the surface are observed in the two negative curvatures at the critical point of the bonds on the top. In the bulk case, the principal axes of the Hessian tensor of the charge density with negative curvatures extend from the BCP toward the octahedral (λ_2) and tetrahedral holes (λ_1). Those octahedral holes disappear in the top of the surfaces; consequently the bonds now cap the tetrahedra graphs in a more symmetrical way around the tetrahedral holes. Thus, λ_2 increases its value and now the negative curvatures have comparable magnitude.

5. Conclusion

A simple numerical method for the topologic analysis of ρ-(**r**) (regardless of how it was generated) is implemented for the EXTREME 94 program. The method allows, for example, the study by DFT of complex systems where the electronic correlation is important, regardless of the kind of basis set and the method used to solve the KS equations, and allows the analysis of the resulting density with the topological theory of Bader.

Acknowledgment. The authors want to acknowledge CONICIT of Venezuela (Project S1-95001616) for providing funding for the Gateway 2000 Pentium Pro and Silicon Graphics O2 workstation used in this work.

References and Notes

(1) Lundqvist, S., March, N. H., Eds.; *Theory of the Inhomogeneous Electron Gas*; New York, 1983.

(2) Parr, R. G.; Yang, W. *Density-Functional Theory of Atoms and Molecules*; Oxford University Press: New York, 1989.

(3) . Perdew, J. P.; Chevary, J. A.; Vosko, S. H.; Jackson, K. A.; Pederson, M. R.; Singh, D. J.; Fiolhais, C. *Phys. Rev.* **1992**, *B46*, 6671.

(4) Andzelm, J.; Wimmer, E. *J. Chem. Phys*. **1992**, *96*, 1280. Andzelm, J.; Baker, J.; Scheiner, A.; Wrinn, M. *Int. J. Quantum Chem*. **1995**, *56*, 734.

(5) Jones, R. O.; Gunnanrson, O. *Rev. Mod. Phys.* **1989**, *61*, 689.

(6) Belley, B. *J. Chem. Phys*. **1990**, *92*, 508.

(7) Harris, F. E.; Koures, A. G. *Int. J. Quantum Chem., Quantum Chem. Symp.* **1995**, *29*, 235.

(8) Seminario, J. M.; Politzer, P., Eds.; *Modern Density Functional Theory: A Tool for Chemistry*; Elsevier: New York, 1995.

(9) Ruette, F., Ed. *Quantum Chemistry Approaches to Chemisorption and Heterogeneous Catalysis*; Kluwer Academic Publishers: Boston, 1992.

(10) Bader, R. F. W. *Atoms in molecules: a quantum theory*; Claredon Press: Oxford, 1990.

(11) Bader, R. F. W. *Acc. Chem. Res.* **1985**, *18*, 9.

(12) Wiberg, K. B.; Bader, R. F. W.; Lau, C. D. H. *J. Am. Chem. Soc*. **1987**, *109*, 985.

(13) Boyd, R. J.; Choi, S. C. *Chem. Phys. Lett*. **1985**, *120*, 80.

(14) Popelier, P. L. A.; Bader, R. F. W. *Chem. Phys. Lett.* **1992**, *189*, 542.

(15) Zou, P. F.; Bader, R. F. W. *Acta Crystallogr*. **1994**, *A50*, 714.

(16) Tsirelson, V. G.; Zou, P. F.; Tang, T.-H.; Bader, R. F. W. *Acta Crystallogr*. **1995**, *A51*, 143.

(17) Eberhart, M. E.; Donovan, M. M.; McLaren, J. M.; Clougherty, D. P. *Prog. Surf. Sci.* **1991**, *3*, 1.

(18) Eberhart, M. E.; Clougherty, D. P.; McLaren, J. M. *J. Mater. Res*. **1993**, *8*, 438.

(19) Aray, Y.; Bader, R. F. W. *Surf. Sci*. **1996**, *351*, 233.

(20) Aray, Y. Rosillo, F.; Murgich, J. *J. Am. Chem. Soc*. **1994**, *116*, 10639.

(21) Aray, Y. Rodriguez, J.; Murgich, J.; Ruette, F. *J. Phys. Chem*. **1993**, *97*, 8393.

(22) Aray, Y.; Rodriguez, J. *Can. J. Chem*. **1996**, *74*, 1014.

(23) Bader, R. F. W.; Keith, T. A. Department of Chemistry, McMaster University, Hamilton, Ontario, Canada, 1994.

(24) Gaussian 94, Revision B.3, Frisch, M. J.; Trucks, G. W.; Schlegel, H. B.; Gill, P. M. W.; Johson, B. G.; Robb, M. A.; Cheeseman, J. R.; Keith, T.; A Peterson, G.; Montgomery, J. A.; Raghavachari, K.; Al-Laham, M. A.; Zakrzewski, V. G.; Ortiz, J. B.; Foresman, J. B.; Peng, C. Y.; Ayala, P. Y.; Chen, W.; Wong, M. W.; Andres, J. L.; Replogle, E. S.; Gomperts, R.; Martin, R. L.; Fox, B. J.; Binkley, J. S.; Defrees, D. J.; Baker, J.; Steward, J. O.; Head-Gordon, M.; Gonzalez, C.; Pople, J. A.

(25) Cioslowski, J.; Nanayakkara, A. *Chem. Phys. Lett*. **1994**, *219*, 151.

(26) Popelier, P. L. A. *Chem. Phys. Lett.* **1994**, *228*, 160.

(27) Gatti, C.; Saunders, V. R.; Roetti, C. *J. Chem. Phys*. **1994**, *101*, 10686.

(28) Dovesi, R.; Saunders, V. R.; Roetti, C. Theoretical Chemistry Group: University of Turin, Italy and Daresbury Laboratory, U.K., 1995.

(29) Guo, J.; Ellis, D. E.; Bader, R. F. W.; MacDougall, P. *J. Cluster Sci*. **1990**, *1*, 210.

(30) Dmol/Dsolid, Release 3.0 and 95.0, Biosym/MSI Inc., San Diego, CA, 1995.

(31) Blaha, P.; Schwarz, K.; Dufek, P.; Augustyn, R. Technical University of Vienna, Austria, 1995.

(32) Bader, R. F. W. *Phys. Rev*. **1994**, *B49*, 13348 1994.

(33) Al−Khafaji, A. W.; Tooley, J. R. *Numerical Methods in Engineering Practice*; Holt, Rinehart and Winston, Inc.: New York, 1986.

(34) Becke, A. D. *J. Chem. Phys.* **1988**, *88*, 2547.

(35) Lee, C.; Yang, W.; Parr, R. G. *Phys. Rev*. **1988**, *B37*, 786.

(36) Krishnan, R.; Frisch, M. J.; People, J. A. *J. Chem. Phys*. **1980**, *72*, 4244.

(37) Ashcroft, N. W.; Mermin, N. D. *Solid State Physics*; Holt, Rinehart and Winston, Inc.: New York, 1976.

(38) Perdew, J. P.; Wang, Y. *Phys. Rev.* **1992**, *B45*, 13244.

(39) Blaha, P.; Schwarz, K. *Int. J. Quantum Chem*. **1983**, *23*, 1535.

(40) Moruzzi, V. L.; Janak, J. F.; Williams, A. R. *Calculated Electronic Properties of Metals*; Pergamon Press: New York, 1978.

(41) Eberhart, M. E. *Philos. Mag. A* **1996**, *73*, 47.

(42) Hahn, T. *International Tables for Crystallography*; Reidel: Boston, 1983; Vol. A.